Supplementary Materials for

Mixing Entropy-Induced Layering Polydispersity Enables Efficient and Stable Perovskite Nanocrystal Light-Emitting Diodes

Sudhir Kumar[1§], Jakub Jagielski[1§], Tian Tian[1], Nikolaos Kallikounis[1], Wan-Chi Lee[1], and Chih-Jen Shih[1*]

[1] *Institute for Chemical and Bioengineering, Department of Chemistry and Applied Biosciences, ETH Zürich, 8093 Zürich, Switzerland*

* Author to whom all correspondence should be addressed. Email: chih-jen.shih@chem.ethz.ch

§ These authors contribute equally to this work.

This PDF file includes:

Materials and Methods
Table S1 to S3
Figs. S1 to S16

Materials and Methods

1. Synthetic procedures

1.1 Chemicals

Oleic acid (OLA, 90% technical grade, Aldrich), Octylamine (OA, 99%, Aldrich), Lead (II) bromide ($PbBr_2$, 98+%, Acros Organics), Toluene (99.8%, Fisher Chemical), *tert*-butyl alcohol (*t*-BuOH, for analysis, Fisher Chemical), *N,N*-Dimethylformamide (DMF, >99.8%, Aldrich), Ethanol (EtOH, absolute for analysis, Merck), Hydrobromic acid (HBr, 48% in water, Sigma-Aldrich), Methylamine (33% in absolute Ethanol, Acros Organics), Formamidine acetate (99%, Acros Organics), Diethyl ether (>99.8%, Thommen-Furler AG). All chemicals listed above were used without any further treatment.

1.2 Synthesis of MABr and FABr precursors

Methylammonium bromide (MABr) was synthesized using the synthetic procedure reported by Pathak et al.[1]. MABr was synthesized by mixing 10 mL of methylamine (33% in EtOH) with 7.5 mL of HBr (48% in H_2O) in 100 mL EtOH. The reaction mixture was stirred for 60 min under ambient conditions and followed by removal of the solvent at 60 °C by means of rotary evaporator. The resulting solid was washed several times with diethylether and recrystallized with EtOH. Finally the purified powder was dried overnight in vacuum oven at 60 °C. Formamidinium bromide (FABr) was synthesized according to the synthetic route developed by Eperon et al.[2] Formamidine acetate was dissolved in 2 molar equivalents of HBr (48% in H_2O) and left under stirring for 10 min at 50 °C. The solvent was removed at 100 °C by means of rotary evaporator. The resulting solid was washed several times with diethylether and recrystallized with EtOH followed by drying in vacuum oven at 60 °C.

1.3 Synthesis of perovskite CQWs

The 2D perovskites, $FAPbBr_3$ and $MAPbBr_3$ were synthesized using modified synthetic route reported in our earlier report.[3-4] Briefly, the perovskite precursors, FABr and MABr (0.53 M) were distinctly dissolved in ethanol, while $PbBr_2$ (0.4 M) was dissolved in polar *N,N*-dimethylformamide (DMF) solvent. OLA (625 μL) and OA (25 μL) were mixed with non-polar solvent (Toluene, 12.5 mL). Both FABr and MABr solutions were premixed in different proportion before final reaction. Subsequently, the precursor solutions mentioned above were added dropwise (375 μL of FA/MA stoichiometric solution and 625 μL of $PbBr_2$) to a non-polar toluene solution consisting long chain organic surfactants, OA as long chain ligand and OLA as stabilizer under constant stirring. An instantaneous colloidal crystallization is triggered due to poor solubility of perovskite precursors in nonpolar toluene. A precipitate is formed immediately and is separated from the reaction mixture by means of centrifugation. The resultant supernatant is discarded and the precipitate containing $FA_xMA_{1-x}PbBr_3$ perovskite CQWs is dispersed in 2.5 mL of fresh toluene, which results the final product.

2. Photophysical Characterization

2.1 Absorption spectra of perovskite CQWs superstructures were collected using a JASCO V670 spectrometer.

2.2 Photoluminescence (PL) spectra and absolute PLQY were recorded with Hamamatsu CCD spectrometer (wavelength resolution < 2 nm). The absolute PLQYs in colloidal solutions (in toluene) and spin-casted thin films were determined using the Quantaurus QY (C11347-11) from Hamamatsu equipped with 150 W xenon light source and a 3.3 inches integrating sphere, which is coated with highly reflective Spectralon. Fig. S2 shows the schematic procedure and estimation principle to measure the absolute PLQYs.

2.3 Time resolved photoluminescence (TRPL) spectra of perovskite CQWs ($FA_nMA_{1-n}PbBr_3$) with varying x component from 0 to 1, a regular interval of 0.2, were performed using a Hamamatsu Quantaurus-Tau (Q-τau) Fluorescence Lifetime Spectrometer (C11367-31) equipped with a photon counting measurement system. The samples were exited using a 365 nm and 470 nm pulsed emission with repetition rate of 500 kHz and 1 MHz.

2.4 X-rays diffraction (XRD) patterns of 2D perovskites were collected using a PANalytical X'Pert PRO-MPD diffractometer with Cu-Kα radiation. The data were recorded in the range of 5-70° 2θ at room temperature with an angular step size of 0.05° and a counting time of 0.23 seconds per step.

2.5 Transmission electron microscopy (TEM) images of perovskite CQWs were captured in cryogenic conditions using STEM (Hitachi HD 2700) equipped with cryo-holder (liquid nitrogen) with high beam acceleration voltages from 80 to 200 kV. Room temperature TEM images were acquired using Titan Krios FEG TEM.

2.6 Scanning electron microscopy (SEM) was utilized to obtain the cross-section image of LED device and surface morphologies of pure $FA_{0.5}MA_{0.5}PbBr_3$ and $FA_{0.5}MA_{0.5}PbBr_3$ + PMMA complex emissive layers using Zeiss ULTRA 55 plus SEM operated at 5 kV and 2 kV, respectively.

2.7 Surface profiler (DektakXT Bruker) was used to evaluate the film thickness of various device layers.

3. Materials, Fabrication, and Characterization of LED Devices

3.1 Materials: Indium tin oxide (ITO) coated glass substrates with a sheet resistance of 15 Ω/□ are purchased from Lumtech Corp. The hole injection material poly(3,4-ethylene-dioxythiophene)-poly(styrene sulfonate) (PEDOT:PSS, Clevios AI 4083) is purchased from Heraeus. Highly pure GPC grade hole transporting materials, poly[*N*,*N'*-bis(4-butylphenyl)-*N*,*N'*-bis(phenyl)-benzidine] (Poly-TPD), poly(9-vinylcarbazole) (PVK), and poly[(9,9-dioctylfluorenyl-2,7-diyl)-co-(4,4'-(*N*-(4-sec-butylphenyl) diphenylamine)] (TFB), 4,4'-Bis(*N*-carbazolyl)-1,1'-biphenyl (CBP), and *N*,*N'*-Di(1-naphthyl)-*N*,*N'*-diphenyl-(1,1'-biphenyl)-4,4'-diamine (NPB) are supplied by Lumtech Corp. The neutral host matrix poly methyl methyacrylate (PMMA, average M. W. 350,000) is purchased from Sigma-Aldrich. Ultrapure sublimed grade electron transporting materials 2,2',2''-(1,3,5-benzinetriyl)-*tris*(1-phenyl-1-*H*-benzimidazole) (TPBi) and tris(2,4,6-trimethyl-3-(pyridin-3-yl)phenyl)borane (3TPYMB), and 2,4,6-tris[3-(diphenylphosphinyl)phenyl]-1,3,5-triazine (PO-T2T) are procured from Lumtech corp. Lithium fluoride (LiF, 99.98%) is purchased from Lumtech corp. and Acros Organics, respectively. Aluminum (Al) pellets (99.999%) were obtained from Kurt J. Lesker Co. Ltd. Above materials were used as received without any further purification.

3.2 LED fabrication: Patterned ITO coated glass substrates were sequentially washed in the Extran MA02 neutral detergent and deionized (DI) water mixture (1:3), acetone, and isopropanol. The substrates were then treated by oxygen plasma for 10 min. Thereafter, the aqueous PEDOT: PSS was spin-coated onto the plasma-irradiated substrates at a speed of 4000 rpm for 20 s then annealed at 130 ^{o}C for 30 min. in the ambient conditions. All substrates were then transferred into a glovebox for the deposition of successive layers. An optional 0.5 - 4.0 mg ml^{-1} of hole transporting layer (HTL) of Poly-TPD, TFB, PVK, CBP, NPB, and mixture of polymeric and molecular hole transporting materials (in chlorobenzene) was spin-coated on PEDOT:PSS layer at 3000 rpm for 40 s then annealed at 130 ^{o}C for 30 min. The emission layer (EML) was then spin-coated at 2500 rpm for 40 s, which comprised the mixture of PMMA with the perovskite CQWs. All substrates were transferred in the ultrahigh vacuum chamber (upto 8×10^{-8} mbar). Subsequently, a 25 to 50 nm ETL (TPBi, 3TPYMB, and PO-T2T) and 1 nm EIL (LiF) was thermally evaporated on the EML through thermal evaporation. Finally, a 70 nm Al cathode layer was also deposited on the EIL through a shadow mask. Each substrate is designed to realize four pixels, each with an active area of 25 mm^2 as defined by the overlapping between Al and

ITO layers. All the devices were stored in the glove box and characterized under the ambient conditions.
ITO coated 0.2 mm thin polyethylene terephthalate (PET) flexible substrates were purchased from Aldrich. Firstly, 30 × 30 mm substrates were cut from the 150 × 150 mm PET sheets. Standard ITO pattern was prepared using photolithography. The patterned ITO substrates were exposed to oxygen plasma for 10 min. Thereafter, the PEDOT:PSS (4000 rpm for 20 s) and Poly-TPD (3000 rpm for 40 s) were sequentially spin-coated onto the substrates then annealed at 130 ºC for 30 min. after each step. Subsequently, EML, a mixture of perovskite CQWs and dielectric polymer was then spin-coated on the Poly-TPD layer. Then successive layers of 3TPYMB or PO-T2T (45 nm), Liq (3 nm), and 70 nm Al cathode were thermally-evaporated in a high vacuum chamber (8×10^{-8} mbar) with their respective deposition rates of 0.05, 0.02, 0.1-0.3 $nm.s^{-1}$. Similar to glass substrates, each substrate is patterned to realize for device with an active area of 25 mm^2, which is defined by the overlapping between the ITO anode and Al cathode layers.

3.3 LED characterization: Current density-voltage-luminance (*J-V-L*) characteristics of the perovskite LEDs were measured using a Keithley 2400 source meter and Photo Research PR 655 spectroradiometer. The electroluminance (EL) spectra of all the devices were also recorded by using a PR 655 spectroradiometer. The Commission Internationale de I'éclairage (CIE) coordinates of perovskite LEDs were calculated using a calibrated CCD spectrometer (ASEQ LR1-Tv.2). The $\eta_{ext.}$ was calculated as the total number of emitted photons divided by the total number of injected electrons by assuming a Lambertian-type emission pattern. The operational lifetime of PerLED devices was measured using smart Ossila Lifetime System (E642) under a constant current.

3.4 LED device optimization:
A series of experiments were performed to optimize the PeLED based on x = 0.5 perovskite CQW emitter by testing a variety of HTL/ETL materials and thicknesses. The control device with an architecture of ITO/PEDOT:PSS/Perovskite CQWs/ TPBi/LiF/Al shows a η_{CE} of 2.76 cd A^{-1} and a maximum external quantum efficiency of (η_{ext}) of 0.67% with a maximum luminance (L_{max}) of 654 cd m^{-2}. Subsequently, the η_{CE}, η_{ext}, and L_{max} increased to 6.24 cd A^{-1}, 1.51% and 2331 cd m^{-2}, respectively, upon mixing a 7.5±0.5 wt% dielectric polymer, PMMA, in the perovskite EML. Fig. S9 shows the SEM images of pristine $FA_{0.5}MA_{0.5}PbrB_3$ perovskite CQWs and perovskite CQWs – PMMA mixture thin films on the plasma treated silicon oxide (SiO_x) substrates, comprising three different compositions (A) SiO_x / pristine $FA_{0.5}MA_{0.5}PbrB_3$ perovskite CQWs, (B) SiO_x / $FA_{0.5}MA_{0.5}PbrB_3$ perovskite CQWs – PMMA mixture, and (C) SiO_x / PEDOT:PSS / $FA_{0.5}MA_{0.5}PbrB_3$ perovskite CQWs – PMMA mixture. Fig. S9A shows large uncovered patches in the thin film morphology. Whereas, a patch free uniform surface morphology observed in the CQWs – PMMA thin film (Fig. S9B). Moreover, almost defect free uniform surface morphology is achieved in SiO_x / PEDOT:PSS / $FA_{0.5}MA_{0.5}PbrB_3$ perovskite CQWs – PMMA thin film (Fig. S9C). Resultant smooth thin film morphology suppresses the leakage current and results in a higher device efficiency. High device performance (η_{CE} = 8.85 cd A^{-1}, η_{ext} = 2.16%, and L_{max} = 2825 cd m^{-2}) was realized by substituting the TPBi layer with a boron core based 3TPYMB electron transporting material. Further enhancement in the device efficiency is achieved through further optimization of 3TPYMB and Al layer thicknesses. Moreover, our champion device with a 45 nm 3TPYMB and 70 nm Al layers shows a η_{CE} = 30.41 cd A^{-1} and a η_{ext} = 7.37% (η_{PE} = 27.30 lm W^{-1}) at an operational voltage of 3.5 V. We attribute the higher device performance to five key mechanisms: (i) low carrier injection barrier due to energy levels of charge transporting layers, (ii) balance charge carrier injection in the EML, (iii) effective hole and electron confinement, (iv) significantly suppress the non-radiative surface plasmon polariton loss at 3TPYMB and Al cathode interface through optimize ETL thicknesses, and (v) a reasonably thick ETL also minimizes the exciton quenching through Al cathode layer by increasing the distance between EML and Al layer.[5] The device also demonstrates a low turn-on voltage at 2.8 V, which is attributed to low electron injection barrier from 3TPYMB ETL based devices. Typically, the η_{CE} of PeLEDs exhibit large efficiency roll-off, at high luminance, because of strong imbalance charge carrier injection in the EML, which is occurred due to higher hole mobility than that of electron mobility. Nearly 20% roll-off in the η_{CE} was observed at 1000 cd m^{-2}. Interestingly, we observed a considerably low efficiency roll-

off in the LEDs, < 7% roll-off in the η_{CE} and η_{ext}. at 5000 cd m^{-2} and 4.53 V, when a poly-TPD layer is deposited between the PEDOT:PSS and composite EML of PMMA and perovskite CQWs. The significantly low-efficiency roll-off is achieved because of two critical factors, first, poly-TPD possessed a higher hole mobility and facilitates more balance charge carrier injection, and second, poly-TPD enables an adequate energy barrier to confine the injected electrons and expedites effective carrier recombination in the EML. Besides, the device illustrates very stable EL spectra with a peak emission at 528 nm through different operational voltages (Fig S11).

The operational lifetime of colloidal nanocrystals based PeLEDs remains a central challenge to utilize these emitters in display devices. Here, we studied lifetime (LT_{50}) of encapsulated PeLED device under a constant driving current using an architecture of ITO/PEDOT:PSS/Poly-TPD/Perovskite CQWs + PMMA/3TPYMB/LiF/Al. Most interestingly, the device shows very stable EL peak at 528 nm before and after the operational lifetime test.

Moreover, an electron transporting material, PO-T2T, with a high thermal stability (T_d = 460 ºC) and nearly two order of magnitude higher electron mobility, 1.7 × 10^{-3} cm^2.V^{-1}s^{-1}, than the 3TPYMB (T_d = 230 ºC and μ_E = 10^{-5} cm^2 V^{-1}s^{-1}) counterpart.[6-7] We observed a sub-bandgap turn-on voltage (V_{on}) of 2.2 V and an average η_{CE} of ~19 cd A^{-1} (Fig. S15). Low V_{on} is attributed to high electron mobility and low lying LUMO energy level that possessed a low electron injection barrier from cathode layer. Most interestingly, the resultant perovskite LEDs show very stable EL spectrum throughout the voltage range, which is also consistent with the 3TPYMB based device. Later on, the operational stability of perovskite CQWs based LEDs is measured at 10 mA cm^{-2} and result a significantly high LT_{50} of 184 min. An unencapsulated device was also tested at L_0 = 74 cd m^{-2} (J = 0.84 mA cm^{-2}), showing an LT_{10} value of 262 minutes (Fig. S16), which is one of the highest value for the unencapsulated perovskite LEDs.

Lastly, we fabricate highly flexible conformable and large area LEDs based on x = 0.5 perovskite CQWs. The EL spectra remain intact throughout the operation voltage that varies from 3.0 to 5.5 V (Fig. S12). A large-area flexible device (225 mm^2) shows commendable stability under both positive and negative bending conditions. On the other hand, a large-area (400 mm^2) device, with the optimized device structure (Fig. S13), shows high performance as well. The device also shows an EL emission at 528 nm, which is strongly consistent with our standard 25 mm^2 device.

4. Energy Transfer Modeling

4.1 ET Efficiency Model:

Under the assumptions that: (i) all emission comes from n = 7 CQWs and (ii) the quantum yields for n = i CQWs are constant and independent of wavelength, the quantum yield as a function of excitation wavelength is given by:

$$\eta_{\mathrm{PL}}(\lambda_{\mathrm{ex}}) = \eta_{\mathrm{PL},n=7}\left[\left(\sum_{i=1}^{6}\mathrm{Abs}_{n=i}(\lambda_{\mathrm{ex}})\eta_{\mathrm{ET},n=i}\right) + \mathrm{Abs}_{n=7}(\lambda_{\mathrm{ex}})\right]\Big/\left(\sum_{i=1}^{7}\mathrm{Abs}_{n=i}(\lambda_{\mathrm{ex}})\right)$$

where $\mathrm{Abs}_{n=i}(\lambda)$ and $\eta_{\mathrm{PL},n=i}$ are the absorption and quantum yield for intrinsic $n = i$ CQW, respectively, and $\eta_{\mathrm{ET},n=i}$ is the energy transfer efficiency from $n = i$ to n = 7 CQW. Accordingly, we can determine $\eta_{\mathrm{ET},n=i}$. And since we obtained nearly wavelength-independent quantum yields, as well as considerable absorption from the donor CQWs, we determine $\eta_{\mathrm{ET}} \sim 1$.

4.2 ET Kinetic Model:

We consider the following kinetics to calculate the emission events resulting from energy transfer from the donor (D; n = 1, 3, and 4) to the acceptor (A; n = 7) CQWs.

$$D^* + A \xrightarrow{k_{\mathrm{ET}}} D + A^*$$

$$A^* \xrightarrow{k_{RA}} A + hv$$

where the superscript * represents photoexcited species, $k_{ET} = 1/\tau_{ET}$ and $k_{RA} = 1/\tau_{RA}$, corresponding to the rate constants for ET and radiative emission of the acceptor, respectively (see main text). The photon generation events I_{ETPL} is therefore given by:

$$I_{ETPL} = \beta \frac{k_{ET}}{k_{RA} - k_{ET}} [\exp(-k_{ET}t) - \exp(-k_{RA}t)]$$

where β is a constant, proportional to the absorbance of the acceptor CQWs. The time required to reach the maximum, t_{max}, is therefore give by:

$$t_{max} = \frac{ln(\frac{k_{RA}}{k_{ET}})}{k_{RA} - k_{ET}}$$

Accordingly, with two fitting parameters, β and k_{ET}, we can least-square fit the experimentally-obtained ET PL response, allowing us to determine t_{max} and τ_{ET}.

Note that if the energy transfer involves photon emission from the donor CQWs (DRET), the kinetics may be also written as:

$$D^* \xrightarrow{k_{RD}} D + hv$$
$$hv + A \xrightarrow{k_{ET}} A^*$$
$$A^* \xrightarrow{k_{RA}} A + hv$$

Accordingly, the photon generation events I_{ETPL} is given by:

$$I_{ETPL} = \beta \frac{k_{RD}k_{ET}}{(k_{ET} - k_{RD})} \left\{ \left[\frac{\exp(-k_{RD}t) - \exp(-k_{RA}t)}{(k_{RA} - k_{RD})} \right] + \left[\frac{\exp(-k_{ET}t) - \exp(-k_{RA}t)}{(k_{RA} - k_{ET})} \right] \right\}$$

corresponding to t_{max} given by:

$$k_{RD}(k_{ET} - k_{RA}) \exp(-k_{RD}t_{max}) + k_{ET}(k_{RA} - k_{RD}) \exp(-k_{ET}t_{max}) + k_{RA}(k_{RD} - k_{ET}) \exp(-k_{RA}t_{max}) = 0$$

We determined τ_{ET} with the former model but in fact the physical pictures in both cases are the same. In addition, the most important conclusion based the calculations, which is the energy transfer mechanism is dominated by the DRET, remains hold for both kinetic models.

Supplementary Tables

Table S1. Summary of perovskite LED characteristics in literature.

V_T (V)	η_{CE} (cd/A)	$\eta_{ext.}$ (%)	λ_{EL} (nm)	Emitter	Reference
Colloidal Nanocrystals and Quantum Dots					
2.60	18.80	8.73	513	$CsPbBr_3$	8
3.4	13.30	6.27	512	$CsPbBr_3$	9
3.1	11.49	3.80	512	$MAPbBr_3$	10
2.9	--.--	10.67	524	$MAPbBr_3$	11
2.75	13.02	3.04	529	$FAPbBr_3$	4
3.2	8.10	2.31	520	$MAPbBr_3$	3
2.8	7.96	3.79	519	$CsPbBr_3$	12
3.4	15.50	5.09	522	$MAPbBr_3$	13
2.5	14.20	4.40	512	Ce^{3+}-doped $CsPbBr_3$	14
3.5	10.09	2.80	526	$FA_{0.8}Cs_{0.2}PbBr_3$	15
3.0	8.50	3.00	515	$CsPbX_3$ (X = Br, Cl)	16
4.6	8.98	2.21	527	$CsPbBr_3$ – $CsPb_2Br_5$	17
2.5	2.25	2.39	522	$CsPbBr_3$	18
Quasi-2D perovskites (Ruddlesden-Popper Phase)					
3.0	--.--	7.00	526	$MAPbBr_3$ + PEABr	19
3.0	62.43	14.36	532	$(PEA_2(FAPbBr_3)_{n-1}PbBr_4$ (n = 2, 3, 4, 5, 6)	20
3.6	4.90	--.--	520	MPEA16($MAPbBr_3$+$(PEA)_2PbBr_4$)	21
3.0	--.--	7.40	526	$PEA_2MA_{n-1}PbBr_{3n+1}$ (n = 5)	22
2.2	--.--	0.10	518	$NFPb_7$ (NMABr: FABr:$PbBr_2$)	23
3.0	6.16	1.97	511	PEABr + $CsPbBr_3$ (0.8 : 1)	24
Bulk perovskite film					
2.8	31.20	10.40	514	$CsPbBr_3$ TCQW	25
3.6	17.10	9.30	513	20:100 (BABr:$MAPbBr_3$)	26
2.8	55.20	12.10	536	$MAPbBr_3$	27
2.2	57.60	13.40	533	2D $(OA)_2(FA)_{n-1}PbnBr_{3n+1}$ & 3D $FAPbBr_3$	28
2.9	33.90	10.43	520	$Cs_{0.87}MA_{0.13}PbBr_3$	29
4.0	42.90	8.53	540	$MAPbBr_3$	30
1.9	22.60	5.70	530	$CsPbBr_3$:PEO:PVP composite film	31
2.8	18.13	6.50	516	OPA-$CsPbBr_3$	32
2.4	23.70	7.30	569	$Cs_{10}(MA_{0.17}FA_{0.83})_{(100-x)}Pb(Br_xI_{1-x})_3$	33
3.6	34.46	8.21	542	$MAPbBr_3$:$PbBr_2$	34
3.4	24.22	7.17	532	7% Rb doped $FAPbBr_3$	35
2.5	15.67	4.26	521	$CsPbBr_3$	36
4.0	15.25	3.38	531	$MAPbBr_3$	37
2.65	45.2	14.40	512	$PEA_2(CsPbBr_3)_{n-1}PbBr_4$	38

Table S2. Photophysical characteristics of $FA_xMA_{1-x}PbBr_3$ perovskite CQWs.

Properties ↓ / x →	Sample type	0	0.2	0.4	0.5	0.6	0.8	1.0
PL (nm)	Solution	520	523	525	527	527	528	530
	Film	521	523	525	527.4	528	529	531
FWHM (nm)	Solution	24.5	24.4	24.0	23.2	24.4	23.2	22.7
	Film	23.6	23.7	23.0	22.7	22.7	22.2	22.0
η_{PL} (%)	Solution	79.0	84.0	87.8	85.7	90.0	91.9	88.0
	Film	86.0	88.6	92.5	99.6	91.7	86.4	94.0

Table S3. Device characteristics of fabricated perovskite NC LEDs as a function of *x*. All data points were taken from same experiment.

$FA_xMA_{1-x}PbBr_3$	V_T (V)	η_{CE} (cd/A)	η_{PE} (lm/W)	η_{ext} (%)	L_{max} (cd/m^2)
		max. / at 1000 cd/m^2			
x = 0.0	2.75	9.41 / 8.22	7.42 / 5.72	2.48 / 2.17	2394
x = 0.2	2.75	15.76 / 14.28	14.15 / 10.93	3.86 / 3.54	2991
x = 0.4	2.75	18.60 / 17.95	16.69 / 14.55	4.55 / 4.42	4575
x = 0.5	2.75	29.72 / 26.46	26.68 / 20.85	7.34 / 6.53	4052
x = 0.6	2.75	22.07 / 21.54	17.34 / 16.47	5.39 / 4.13	3626
x = 0.8	2.75	19.99 / 18.47	17.94 / 15.13	4.92 / 4.54	4964
x = 1.0	2.75	12.76 / 11.34	13.36 / 10.18	3.04 / 2.74	2939

Supplementary Figures

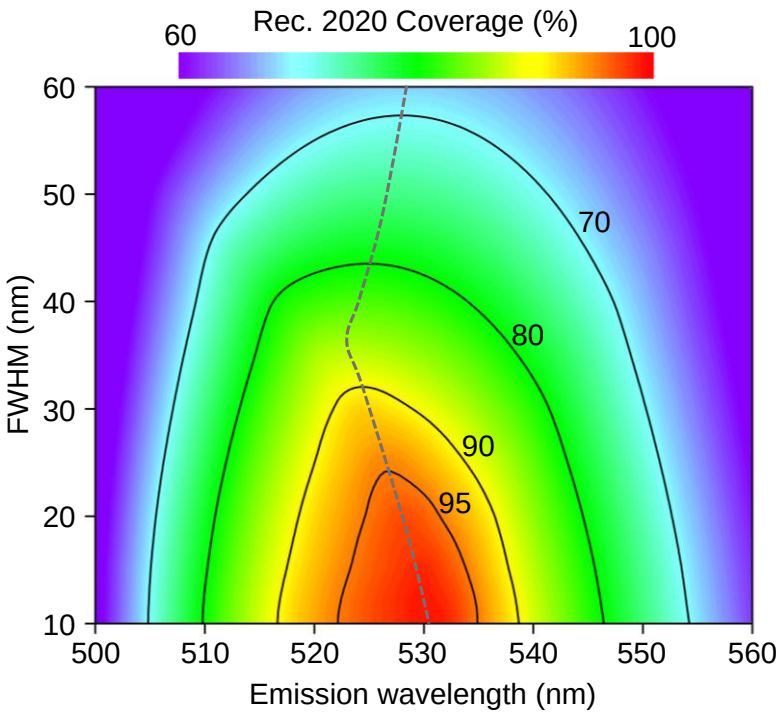

Figure S1. Calculated color gamut coverage on the Rec. 2020 as a function of emission wavelength and FWHM. The dashed line corresponds to the optimal emission wavelength as a function of FWHM.

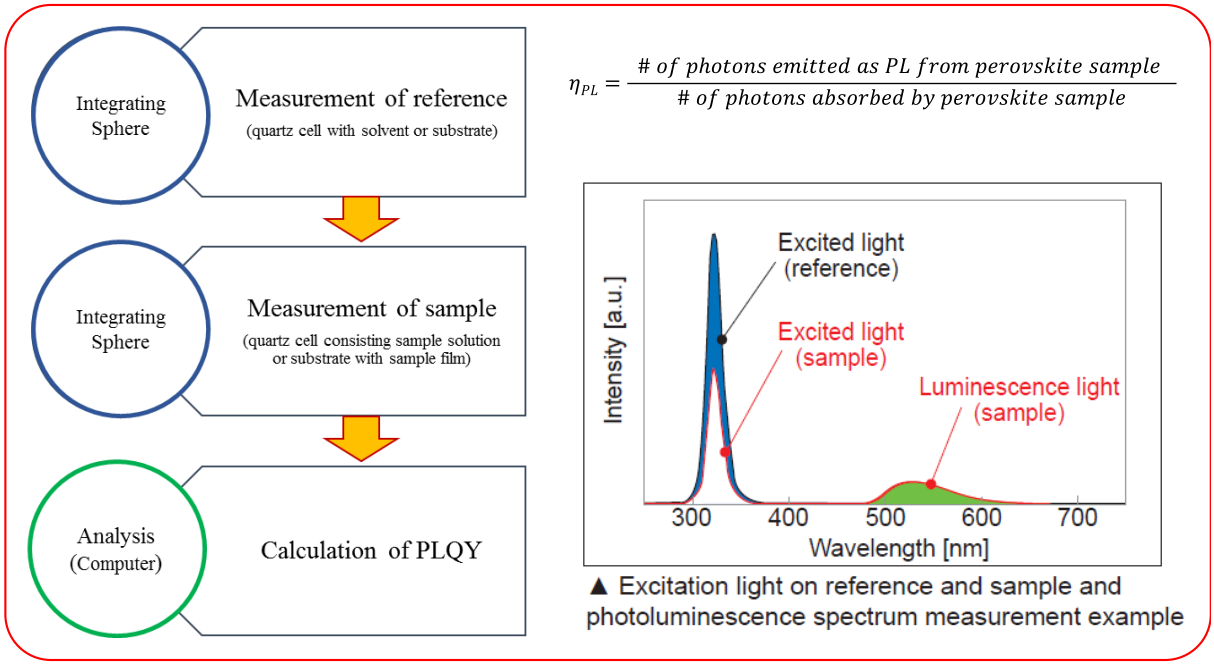

Figure S2. Schematic presentation of measurement procedure (left) and principle of absolute PLQY calculation (right) measured by Hamamatsu Quantaurus-QY (C11347-11).

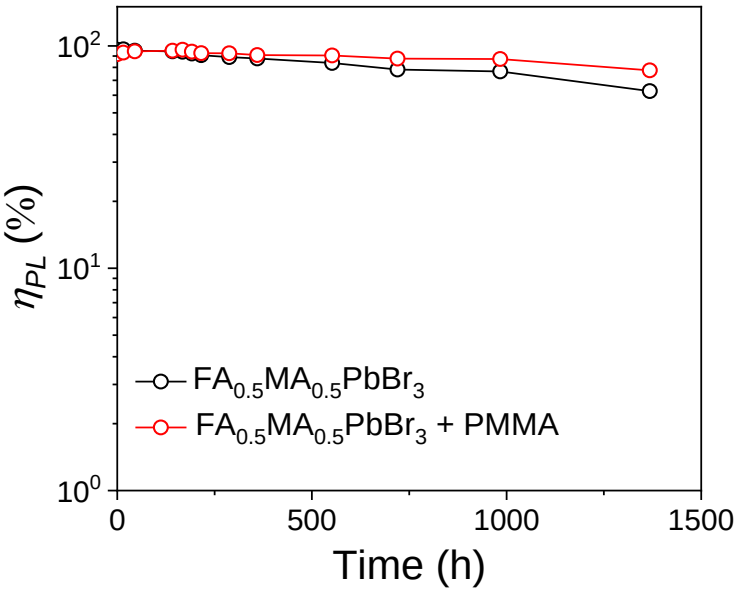

Figure S3. The measured thin-film η_{PL} values of pure $FA_{0.5}MA_{0.5}PbBr_3$ and PMMA capped $FA_{0.5}MA_{0.5}PbBr_3$ as a function of time showing excellent air stability (~50% RH) at room temperature.

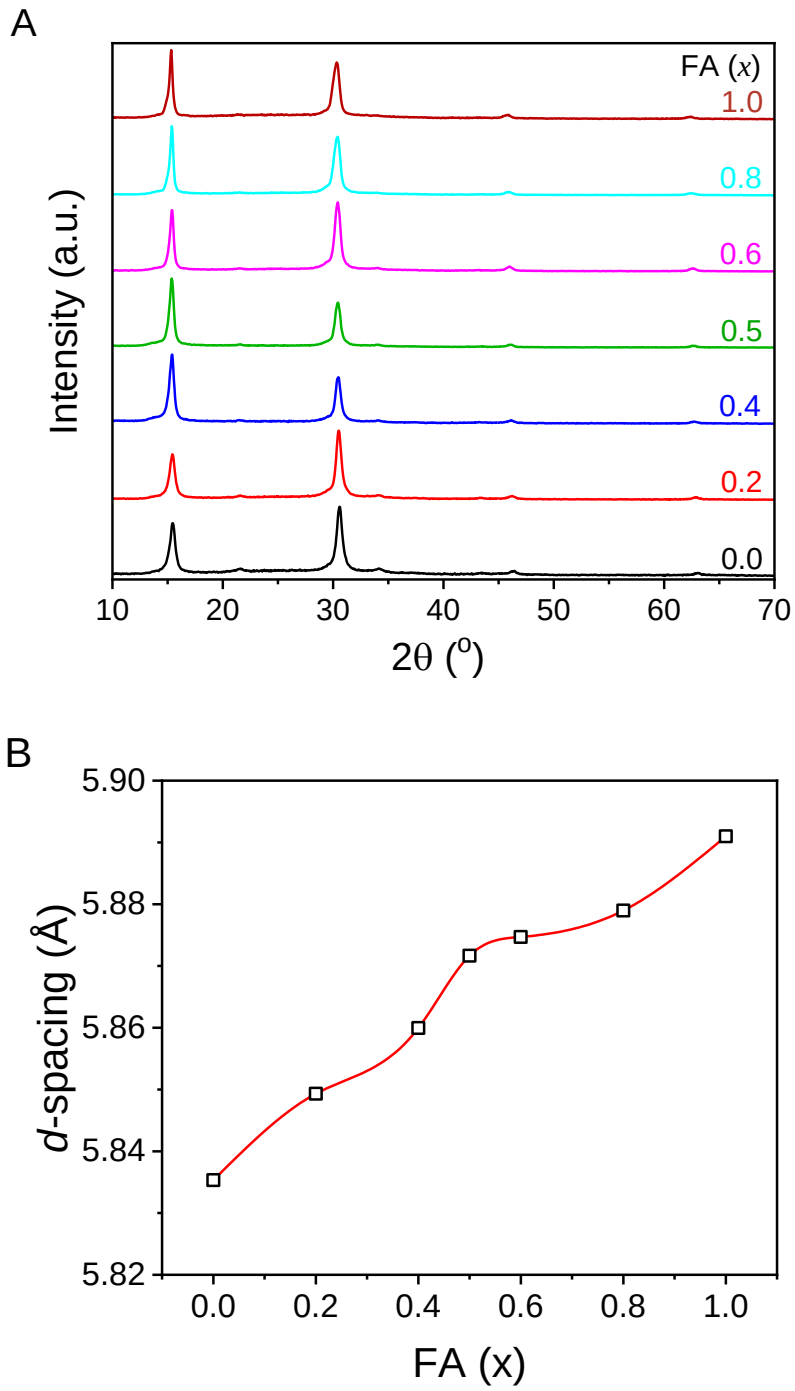

Figure S4. (A) X-ray diffraction patterns of perovskite ($FA_xMA_{1-x}PbBr_3$) CQWs as FA content (*x*) from 0 to 1. **(B)** Average *d*-spacing in perovskite CQWs as a function of FA content (*x*) from 0 to 1.

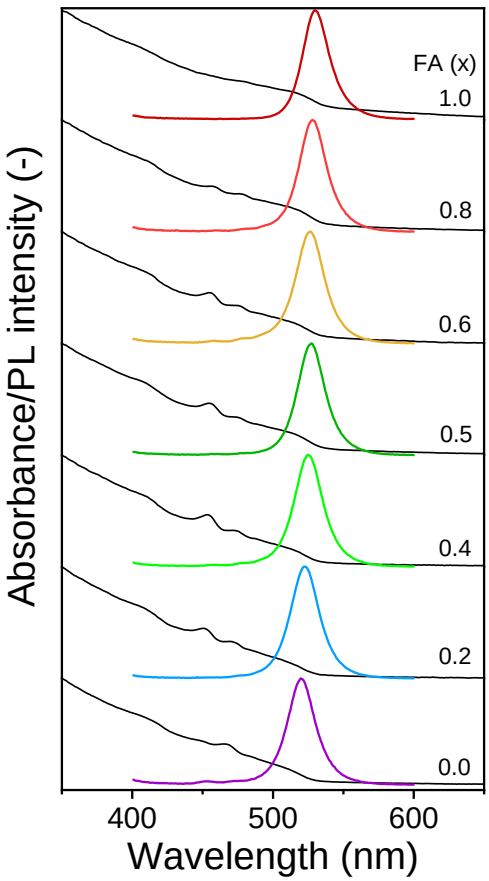

Figure S5. Absorption and PL spectra for $FA_xMA_{1-x}PbBr_3$ CQW superstructures at *x* values varying from 0 to 1.

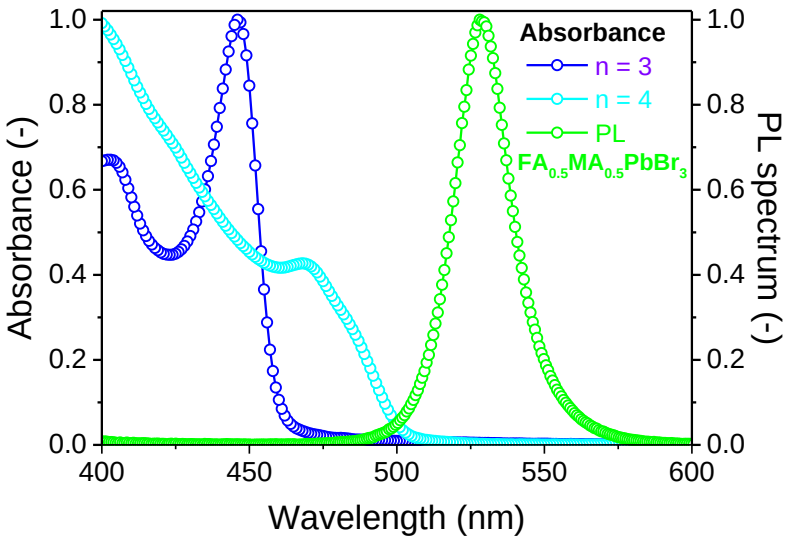

Figure S6. Absorption spectra of pure n = 3 and 4 layers colloidal NC assemblies and PL spectrum of polydisperse colloidal NC assemblies with a composition of $FA_{0.5}MA_{0.5}PbBr_3$ perovskite.

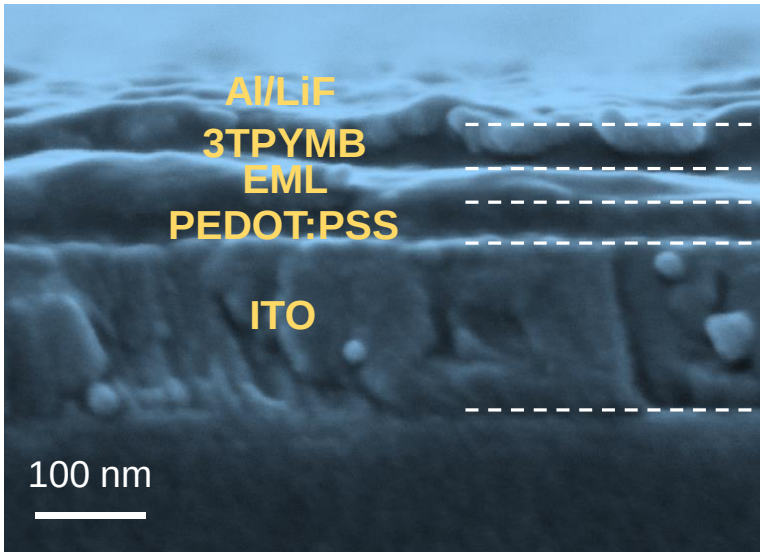

Figure S7. Cross-sectional SEM image of our perovskite NC LED.

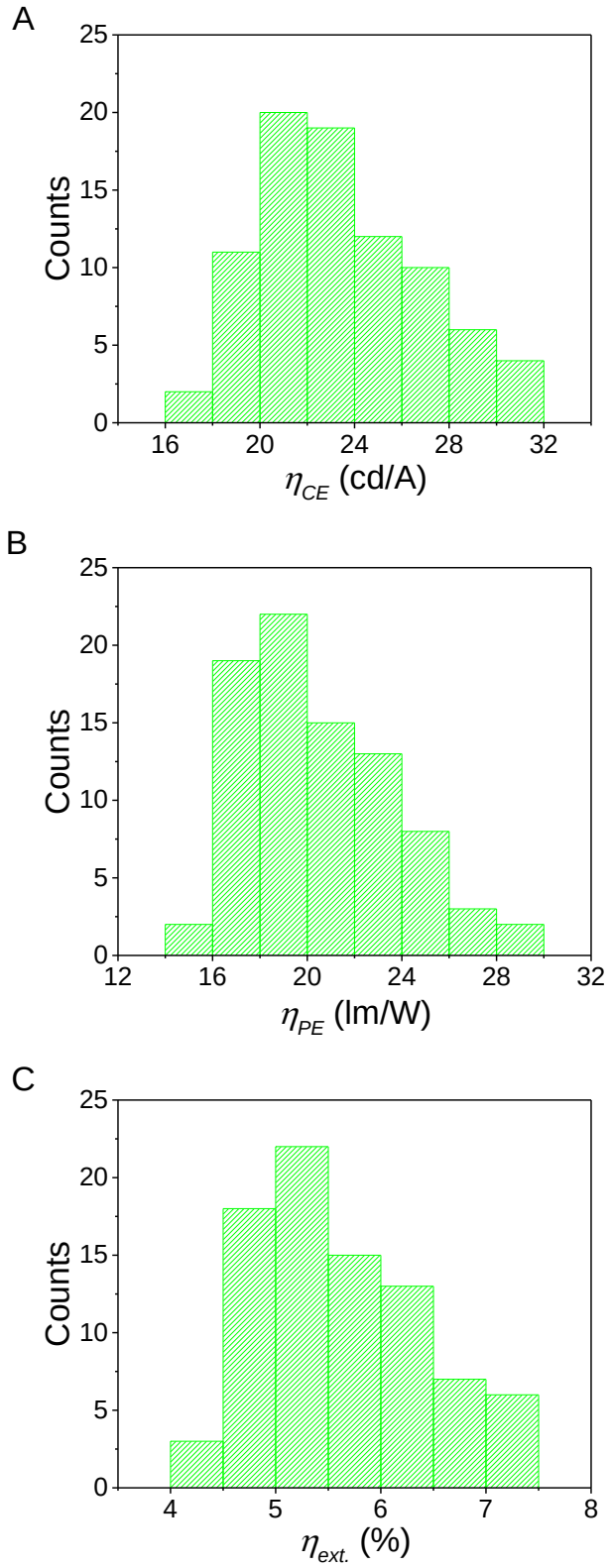

Figure S8. Histograms of maximum **(A)** current efficiencies, **(B)** power efficiencies, and **(C)** external quantum efficiencies measured from 84 PerLEDs with the optimized device structure.

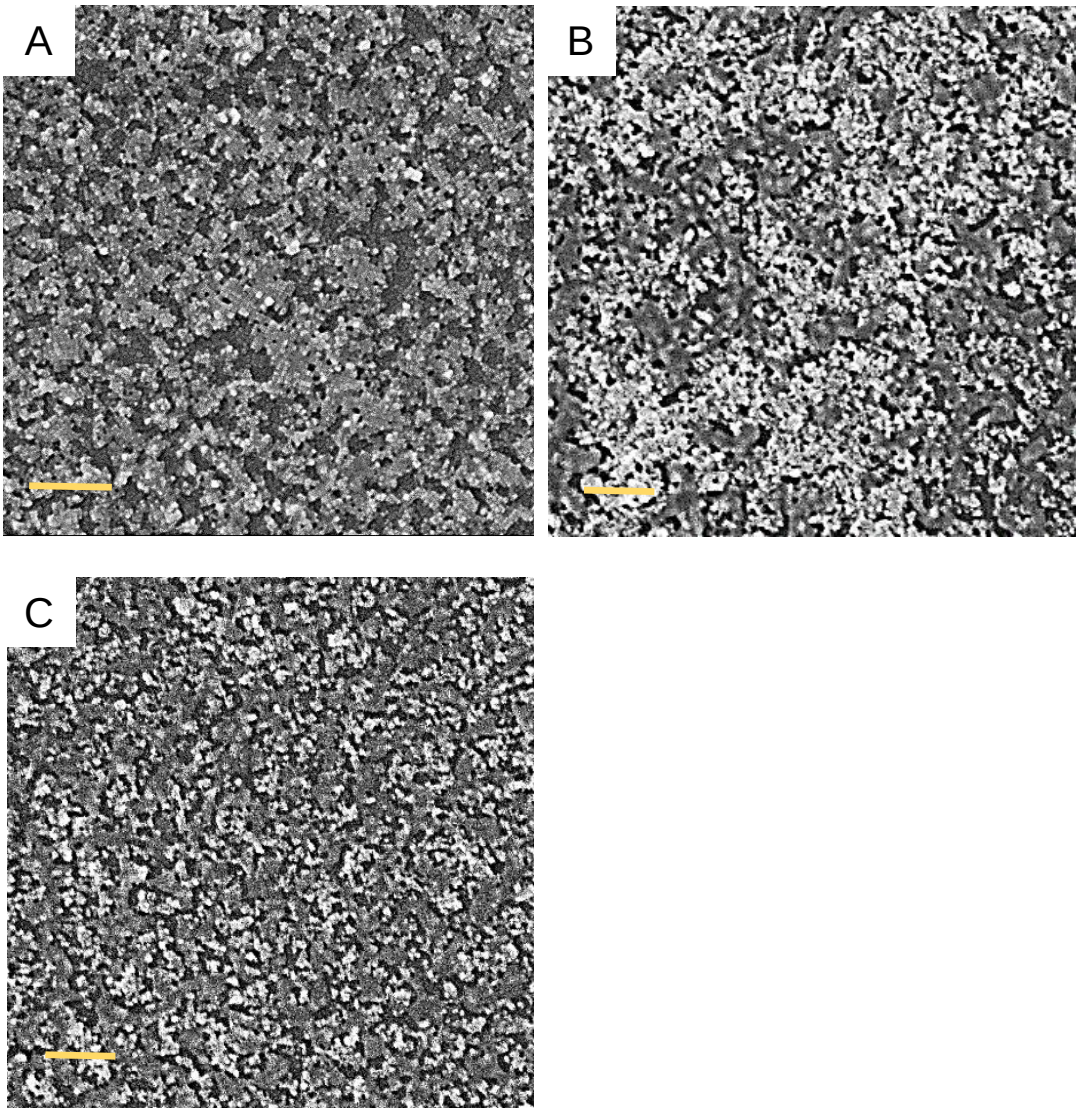

Figure S9. SEM images of (A) pristine $FA_{0.5}MA_{0.5}PbrB_3$ perovskite CQWs spin-casted thin film on plasma-treated silicon oxide wafer, (B) $FA_{0.5}MA_{0.5}PbrB_3$ perovskite CQWs - PMMA complex thin film on plasma treated silicon oxide wafer, and (C) $FA_{0.5}MA_{0.5}PbrB_3$ perovskite CQWs - PMMA complex on PEDOT:PSS coated silicon oxide wafer. The PEDOT:PSS layer is annealed at 130 ºC for 30 minutes before spin-casting the perovskite CQWs - PMMA emissive layer. The scale bar is 100 nm.

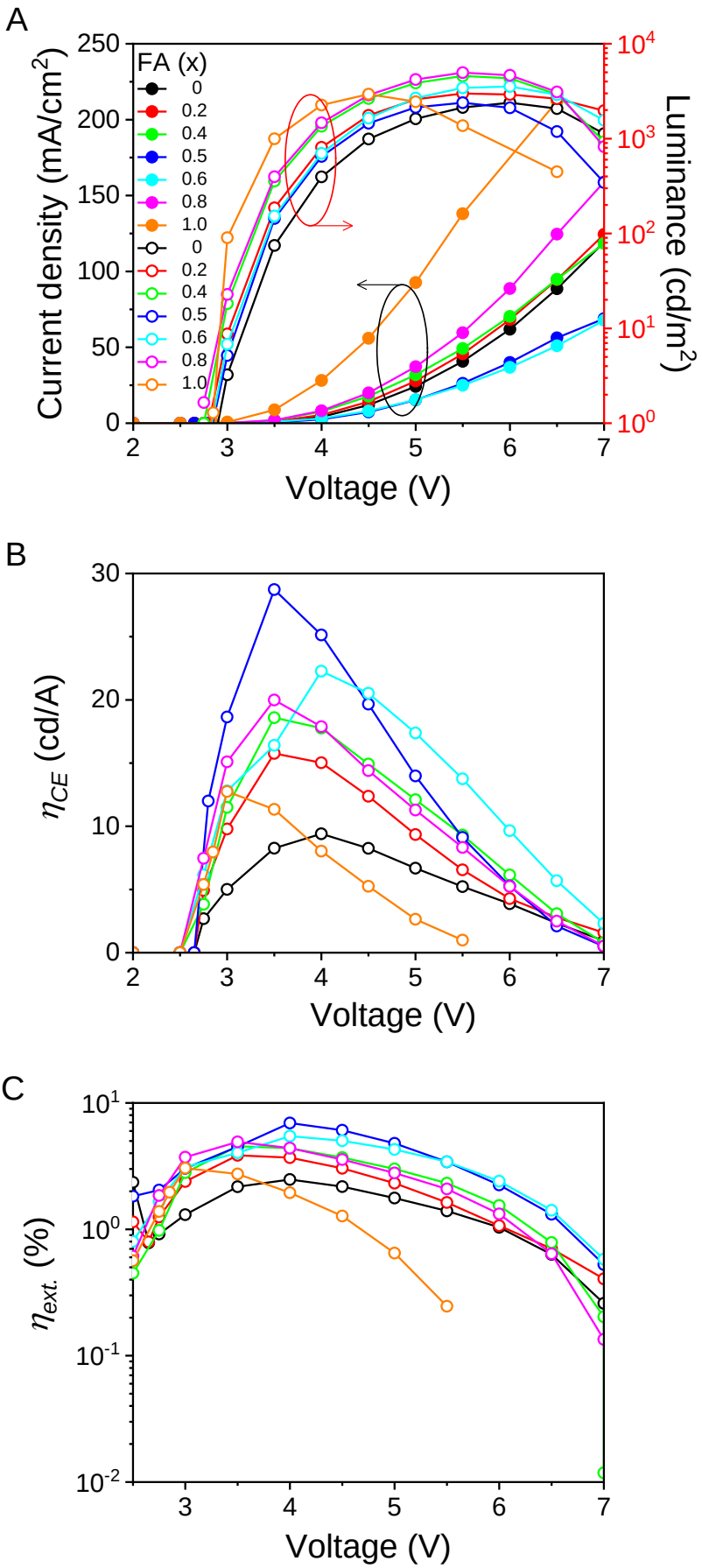
A
FA (x)
0
0.2
0.4
0.5
0.6
0.8
1.0
0
0.2
0.4
0.5
0.6
0.8
1.0
Current density (mA/cm2)
Luminance (cd/m2)
Voltage (V)
B
ηCE (cd/A)
Voltage (V)
C
ηext. (%)
Voltage (V)

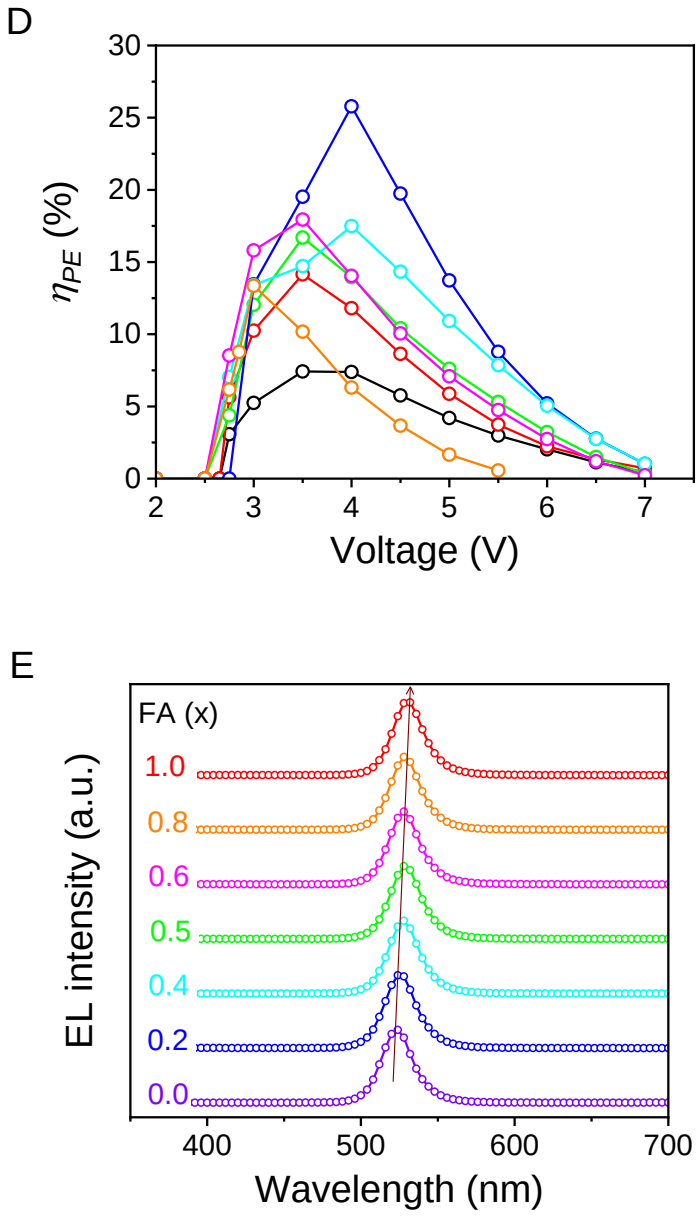

Figure S10. (**A**) Current-density and luminance as a function of driving voltage. (**B**) Current efficiency as a function of driving voltage. (**C**) EQE as a function of driving voltage. (**D**) Power efficiency as a function of driving voltage. (**E**) EL spectra for various x values considered here.

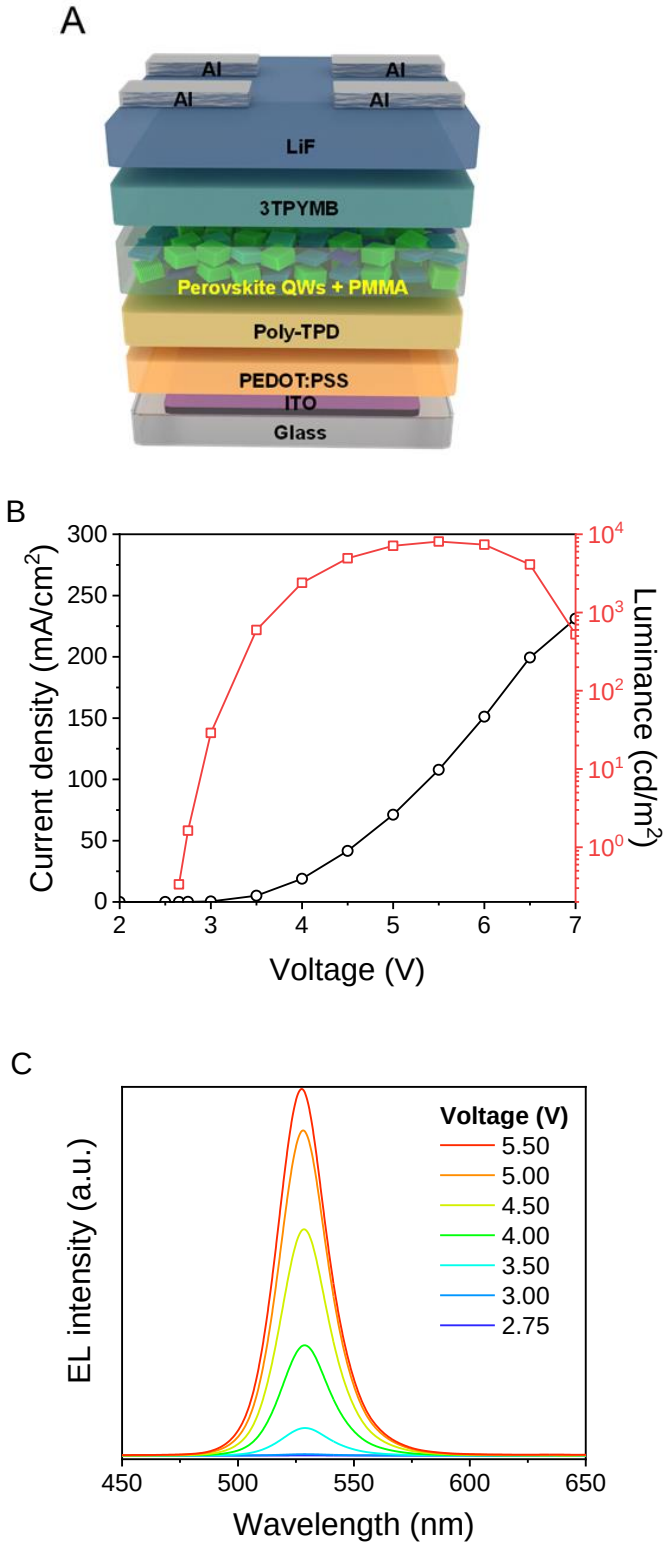

Figure S11. (**A**) Schematic device architecture with ITO / PEDOT:PSS / Poly-TPD / EML (Perovskite CQWs + PMMA) / 3TPYMB / LiF / Al. (**B**) Current-density-voltage-luminance (*J-V-L*) characteristics, (**C**) EL spectrum of LED device for driving voltages of 2.75 to 5.50 V.

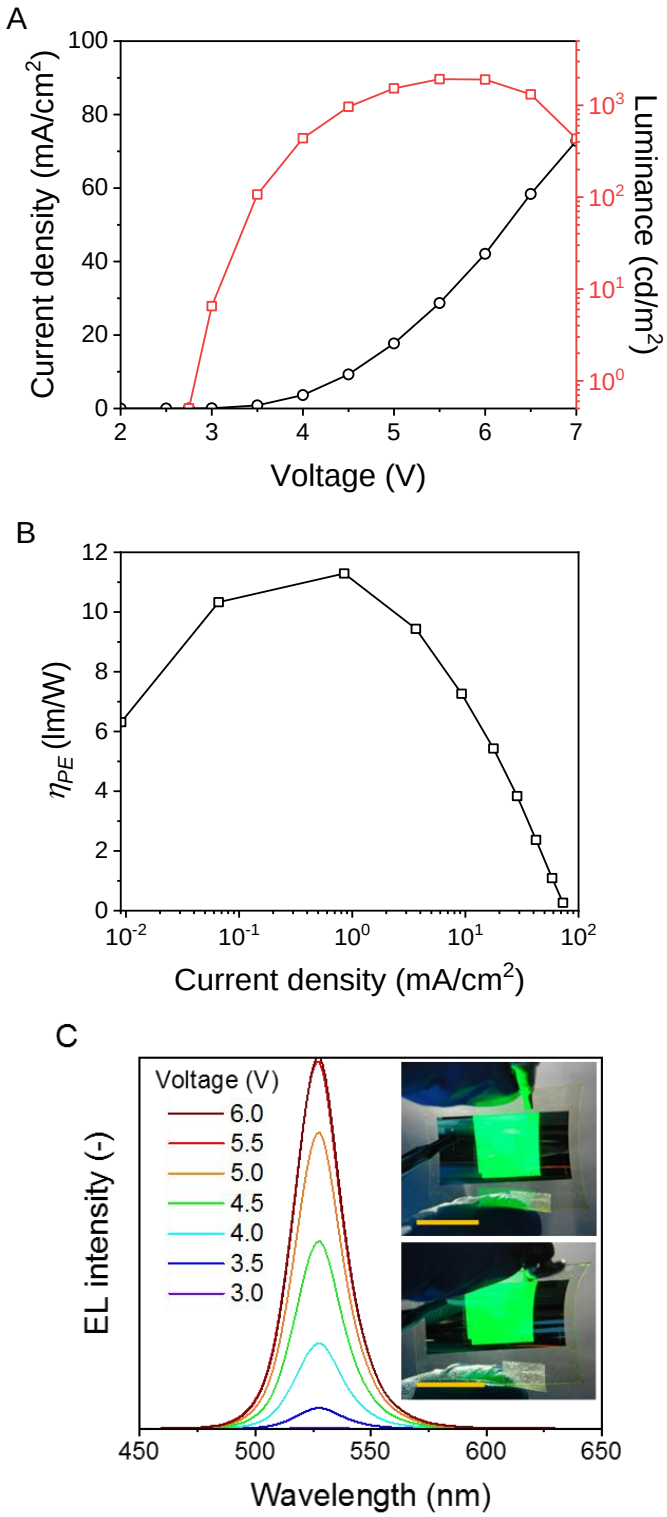

Figure S12. Flexible LED devices. (**A**) Current density and luminance as a function of voltage. (**B**) Power efficiency (η_{PE}) as a function of current density. (**C**) EL spectra of device at different driving voltages. Inset: Photographs of a 400 mm^2 large area flexible LED at 4.5 V with a positive (top right) and negative (bottom right) bending radii of ~8±0.5 mm (scale bar: 15 mm).

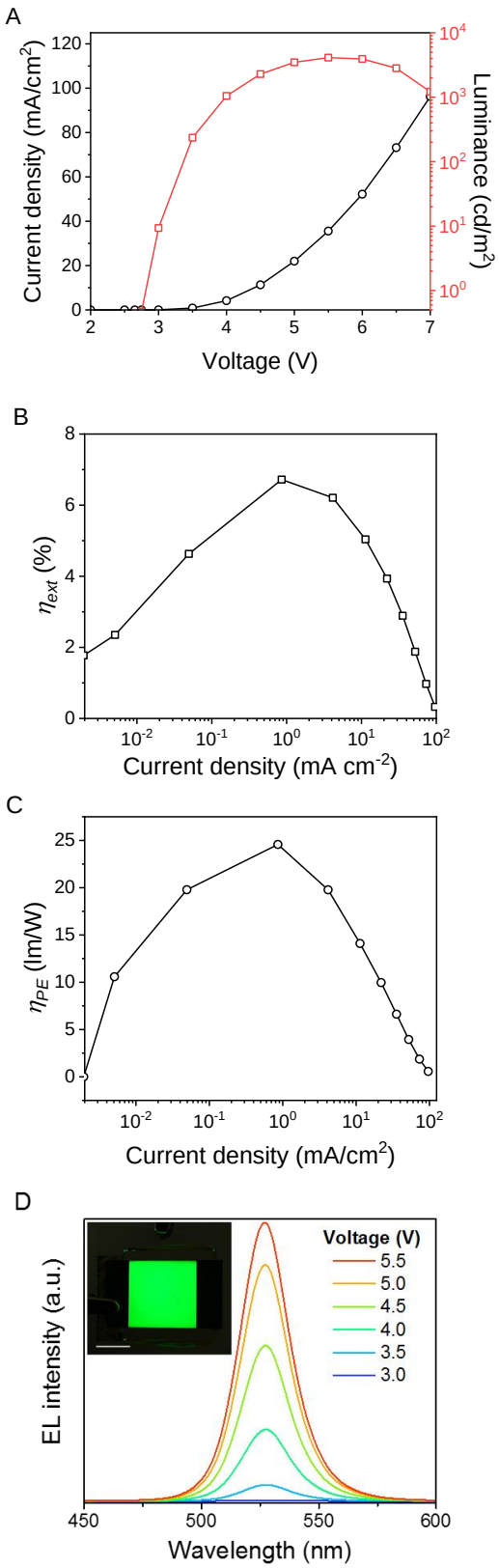

Figure S13. Large-area LED devices. (**A**) Current-density and luminance as a function of driving voltage, (**B**) EQE (η_{ext}) as a function of current density, (**C**) Power efficiency (η_{PE}) as a function of current density, and (**D**) EL spectra at voltages of 3 to 5.5 V. Inset: Photographs of a 400 mm^2-large LED at 3.5 V (scale bar: 10 mm).

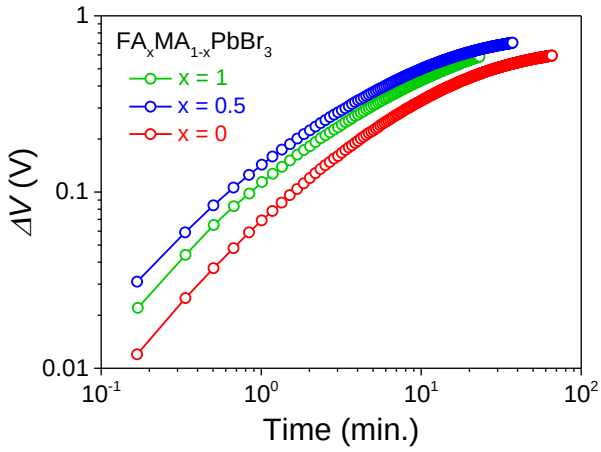

Figure S14. Driving voltage change as a function of time under continuous electrical stress at a constant current density of 20 mA cm^{-2}.

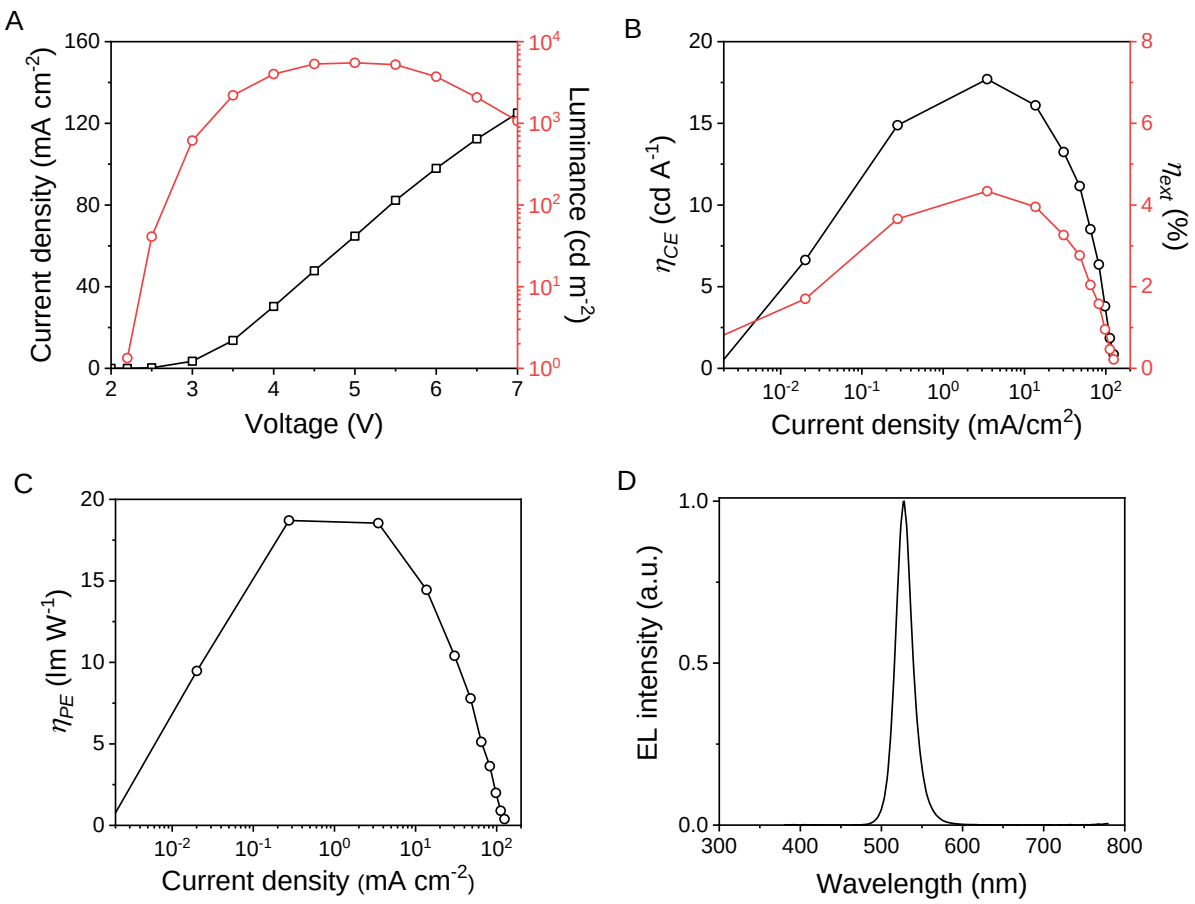

Figure S15. Perovskite LEDs using polydisperse CQWs at x = 0.5 and PO-T2T electron transporting layer. (A) *J-V-L* characteristics. (B) Current efficiency and external quantum efficiency as a function of current density. (C) Power efficiency as a function of current density. (D) EL spectrum.

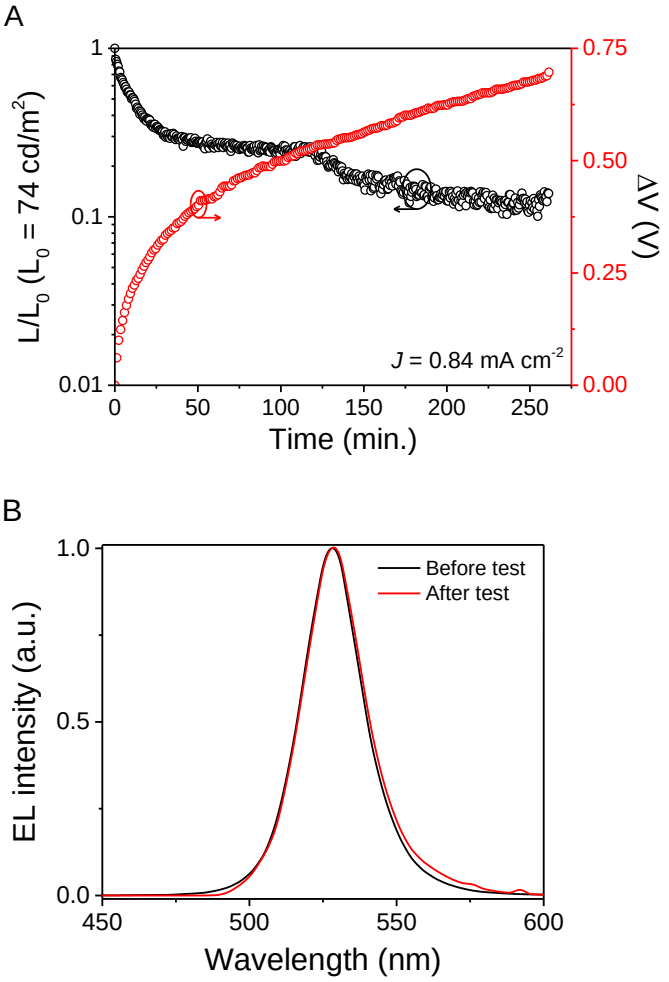

Figure S16. Operational Lifetime test for an unencapsulated device, (**A**) Relative luminance and driving voltage change, and (**B**) EL spectra of device before and after lifetime test.

References

1. Pathak, S.; Sakai, N.; Rivarola, F. W. R.; Stranks, S. D.; Liu, J. W.; Eperon, G. E.; Ducati, C.; Wojciechowski, K.; Griffiths, J. T.; Haghighirad, A. A.; Pellaroque, A.; Friend, R. H.; Snaith, H. J., Perovskite crystals for tunable white light emission. *Chemistry of Materials* **2015,** *27* (23), 8066-8075.
2. Eperon, G. E.; Stranks, S. D.; Menelaou, C.; Johnston, M. B.; Herz, L. M.; Snaith, H. J., Formamidinium lead trihalide: a broadly tunable perovskite for efficient planar heterojunction solar cells. *Energy & Environmental Science* **2014,** *7* (3), 982-988.
3. Kumar, S.; Jagielski, J.; Yakunin, S.; Rice, P.; Chiu, Y.-C.; Wang, M.; Nedelcu, G.; Kim, Y.; Lin, S.; Santos, E. J. G.; Kovalenko, M. V.; Shih, C.-J., Efficient blue electroluminescence using quantum-confined two-dimensional perovskites. *ACS Nano* **2016,** *10* (10), 9720-9729.
4. Kumar, S.; Jagielski, J.; Kallikounis, N.; Kim, Y.-H.; Wolf, C.; Jenny, F.; Tian, T.; Hofer, C. J.; Chiu, Y.-C.; Stark, W. J.; Lee, T.-W.; Shih, C.-J., Ultrapure green light-emitting

diodes using two-dimensional formamidinium perovskites: Achieving recommendation 2020 Color Coordinates. *Nano Letters* **2017,** *17* (9), 5277-5284.
5. Jou, J.-H.; Kumar, S.; Agrawal, A.; Li, T.-H.; Sahoo, S., Approaches for fabricating high efficiency organic light emitting diodes. *Journal of Materials Chemistry C* **2015,** *3* (13), 2974-3002.
6. Hung, W.-Y.; Fang, G.-C.; Lin, S.-W.; Cheng, S.-H.; Wong, K.-T.; Kuo, T.-Y.; Chou, P.-T., The First Tandem, All-exciplex-based WOLED. *Scientific Reports* **2014,** *4*, 5161.
7. Tanaka, D.; Takeda, T.; Chiba, T.; Watanabe, S.; Kido, J., Novel electron-transport material containing boron atom with a high triplet excited energy level. *Chemistry Letters* **2007,** *36* (2), 262-263.
8. Chiba, T.; Hoshi, K.; Pu, Y.-J.; Takeda, Y.; Hayashi, Y.; Ohisa, S.; Kawata, S.; Kido, J., High-efficiency perovskite quantum-dot light-emitting devices by effective washing process and interfacial energy level alignment. *ACS Applied Materials & Interfaces* **2017,** *9* (21), 18054-18060.
9. Li, J.; Xu, L.; Wang, T.; Song, J.; Chen, J.; Xue, J.; Dong, Y.; Cai, B.; Shan, Q.; Han, B.; Zeng, H., 50-Fold EQE improvement up to 6.27% of solution-processed all-inorganic perovskite $CsPbBr_3$ QLEDs via surface ligand density control. *Advanced Materials* **2017,** *29* (5), 1603885.
10. Xing, J.; Yan, F.; Zhao, Y.; Chen, S.; Yu, H.; Zhang, Q.; Zeng, R.; Demir, H. V.; Sun, X.; Huan, A.; Xiong, Q., High-efficiency light-emitting diodes of organometal halide perovskite amorphous nanoparticles. *ACS Nano* **2016,** *10* (7), 6623-6630.
11. Yan, F.; Xing, J.; Xing, G.; Quan, L.; Tan, S. T.; Zhao, J.; Su, R.; Zhang, L.; Chen, S.; Zhao, Y.; Huan, A.; Sargent, E. H.; Xiong, Q.; Demir, H. V., Highly efficient visible colloidal lead-halide perovskite nanocrystal light-emitting diodes. *Nano Letters* **2018,** *18* (5), 3157–3164.
12. Shi, Z.; Li, S.; Li, Y.; Ji, H.; Li, X.; Wu, D.; Xu, T.; Chen, Y.; Tian, Y.; Zhang, Y.; Shan, C.; Du, G., Strategy of solution-processed all-inorganic heterostructure for humidity/temperature-stable perovskite quantum dot light-emitting diodes. *ACS Nano* **2018,** *12* (2), 1462-1472.
13. Kim, Y.-H.; Wolf, C.; Kim, Y.-T.; Cho, H.; Kwon, W.; Do, S.; Sadhanala, A.; Park, C. G.; Rhee, S.-W.; Im, S. H.; Friend, R. H.; Lee, T.-W., Highly efficient light-emitting diodes of colloidal metal–halide perovskite nanocrystals beyond quantum size. *ACS Nano* **2017,** *11* (7), 6586-6593.
14. Yao, J.-S.; Ge, J.; Han, B.-N.; Wang, K.-H.; Yao, H.-B.; Yu, H.-L.; Li, J.-H.; Zhu, B.-S.; Song, J.-Z.; Chen, C.; Zhang, Q.; Zeng, H.-B.; Luo, Y.; Yu, S.-H., Ce3+-Doping to modulate photoluminescence kinetics for efficient $CsPbBr_3$ nanocrystals based light-emitting diodes. *Journal of the American Chemical Society* **2018,** *140* (10), 3626-3634.
15. Zhang, X.; Liu, H.; Wang, W.; Zhang, J.; Xu, B.; Karen, K. L.; Zheng, Y.; Liu, S.; Chen, S.; Wang, K.; Sun, X. W., Hybrid perovskite light-emitting diodes based on perovskite nanocrystals with organic–inorganic mixed cations. *Advanced Materials* **2017,** *29* (18), 1606405.
16. Pan, J.; Quan, L. N.; Zhao, Y.; Peng, W.; Murali, B.; Sarmah, S. P.; Yuan, M.; Sinatra, L.; Alyami, N. M.; Liu, J.; Yassitepe, E.; Yang, Z.; Voznyy, O.; Comin, R.; Hedhili, M. N.; Mohammed, O. F.; Lu, Z. H.; Kim, D. H.; Sargent, E. H.; Bakr, O. M., Highly efficient perovskite-quantum-dot light-emitting diodes by surface engineering. *Advanced Materials* **2016,** *28* (39), 8718-8725.
17. Zhang, X.; Xu, B.; Zhang, J.; Gao, Y.; Zheng, Y.; Wang, K.; Sun, X. W., All-inorganic perovskite nanocrystals for high-efficiency light emitting diodes: dual-phase $CsPbBr_3$-$CsPb_2Br_5$ composites. *Advanced Functional Materials* **2016,** *26* (25), 4595-4600.

18. Shi, Z.; Li, Y.; Zhang, Y.; Chen, Y.; Li, X.; Wu, D.; Xu, T.; Shan, C.; Du, G., High-efficiency and air-stable perovskite quantum dots light-emitting diodes with an all-inorganic heterostructure. *Nano Letters* **2017,** *17* (1), 313-321.
19. Zhao, L.; Yeh, Y.-W.; Tran, N. L.; Wu, F.; Xiao, Z.; Kerner, R. A.; Lin, Y. L.; Scholes, G. D.; Yao, N.; Rand, B. P., In situ preparation of metal halide perovskite nanocrystal thin films for improved light-emitting devices. *ACS Nano* **2017,** *11* (4), 3957-3964.
20. Yang, X.; Zhang, X.; Deng, J.; Chu, Z.; Jiang, Q.; Meng, J.; Wang, P.; Zhang, L.; Yin, Z.; You, J., Efficient green light-emitting diodes based on quasi-two-dimensional composition and phase engineered perovskite with surface passivation. *Nature Communications* **2018,** *9* (1), 570.
21. Byun, J.; Cho, H.; Wolf, C.; Jang, M.; Sadhanala, A.; Friend, R. H.; Yang, H.; Lee, T. W., Efficient Visible Quasi-2D Perovskite Light-Emitting Diodes. *Advanced Materials* **2016,** *28* (34), 7515-7520.
22. Quan, L. N.; Zhao, Y.; García de Arquer, F. P.; Sabatini, R.; Walters, G.; Voznyy, O.; Comin, R.; Li, Y.; Fan, J. Z.; Tan, H.; Pan, J.; Yuan, M.; Bakr, O. M.; Lu, Z.; Kim, D. H.; Sargent, E. H., Tailoring the Energy Landscape in Quasi-2D Halide Perovskites Enables Efficient Green-Light Emission. *Nano Letters* **2017,** *17* (6), 3701-3709.
23. Wang, N.; Cheng, L.; Ge, R.; Zhang, S.; Miao, Y.; Zou, W.; Yi, C.; Sun, Y.; Cao, Y.; Yang, R.; Wei, Y.; Guo, Q.; Ke, Y.; Yu, M.; Jin, Y.; Liu, Y.; Ding, Q.; Di, D.; Yang, L.; Xing, G.; Tian, H.; Jin, C.; Gao, F.; Friend, R. H.; Wang, J.; Huang, W., Perovskite light-emitting diodes based on solution-processed self-organized multiple quantum wells. *Nature Photonics* **2016,** *10*, 699.
24. Ng, Y. F.; Kulkarni, S. A.; Parida, S.; Jamaludin, N. F.; Yantara, N.; Bruno, A.; Soci, C.; Mhaisalkar, S.; Mathews, N., Highly efficient Cs-based perovskite light-emitting diodes enabled by energy funnelling. *Chemical Communications* **2017,** *53* (88), 12004-12007.
25. Si, J.; Liu, Y.; He, Z.; Du, H.; Du, K.; Chen, D.; Li, J.; Xu, M.; Tian, H.; He, H.; Di, D.; Lin, C.; Cheng, Y.; Wang, J.; Jin, Y., Efficient and high-color-purity light-emitting diodes based on in situ grown films of CsPbX3 (X = Br, I) nanoplates with controlled thicknesses. *ACS Nano* **2017,** *11* (11), 11100-11107.
26. Xiao, Z.; Kerner, R. A.; Zhao, L.; Tran, N. L.; Lee, K. M.; Koh, T.-W.; Scholes, G. D.; Rand, B. P., Efficient perovskite light-emitting diodes featuring nanometre-sized crystallites. *Nature Photonics* **2017,** *11*, 108.
27. Lee, S.; Park, J. H.; Nam, Y. S.; Lee, B. R.; Zhao, B.; Di Nuzzo, D.; Jung, E. D.; Jeon, H.; Kim, J.-Y.; Jeong, H. Y.; Friend, R. H.; Song, M. H., Growth of nanosized single crystals for efficient perovskite light-emitting diodes. *ACS Nano* **2018,** *12* (4), 3417-3423.
28. Chin, X. Y.; Perumal, A.; Bruno, A.; Yantara, N.; Veldhuis, S. A.; Martinez-Sarti, L.; Chandran, B.; Chirvony, V.; Lo, A. S.-Z.; So, J.; Soci, C.; Gratzel, M.; Bolink, H. J.; Mathews, N.; Mhaisalkar, S. G., Self-assembled hierarchical nanostructured perovskites enable highly efficient LEDs via an energy cascade. *Energy & Environmental Science* **2018,** *11*, 1770-1778.
29. Zhang, L.; Yang, X.; Jiang, Q.; Wang, P.; Yin, Z.; Zhang, X.; Tan, H.; Yang, Y.; Wei, M.; Sutherland, B. R.; Sargent, E. H.; You, J., Ultra-bright and highly efficient inorganic based perovskite light-emitting diodes. *Nature Communications* **2017,** *8*, 15640.
30. Cho, H.; Jeong, S.-H.; Park, M.-H.; Kim, Y.-H.; Wolf, C.; Lee, C.-L.; Heo, J. H.; Sadhanala, A.; Myoung, N.; Yoo, S.; Im, S. H.; Friend, R. H.; Lee, T.-W., Overcoming the electroluminescence efficiency limitations of perovskite light-emitting diodes. *Science* **2015,** *350* (6265), 1222-1225.

31. Li, J.; Shan, X.; Bade, S. G. R.; Geske, T.; Jiang, Q.; Yang, X.; Yu, Z., Single-Layer Halide Perovskite Light-Emitting Diodes with Sub-Band Gap Turn-On Voltage and High Brightness. *The Journal of Physical Chemistry Letters* **2016,** *7* (20), 4059-4066.
32. Tan, Y.; Zou, Y.; Wu, L.; Huang, Q.; Yang, D.; Chen, M.; Ban, M.; Wu, C.; Wu, T.; Bai, S.; Song, T.; Zhang, Q.; Sun, B., Highly Luminescent and Stable Perovskite Nanocrystals with Octylphosphonic Acid as a Ligand for Efficient Light-Emitting Diodes. *ACS Applied Materials & Interfaces* **2018,** *10* (4), 3784-3792.
33. Kim, H. P.; Kim, J.; Kim, B. S.; Kim, H. M.; Kim, J.; Yusoff, A. R. b. M.; Jang, J.; Nazeeruddin, M. K., High-Efficiency, Blue, Green, and Near-Infrared Light-Emitting Diodes Based on Triple Cation Perovskite. *Advanced Optical Materials* **2017,** *5* (7), 1600920.
34. Lee, J.-W.; Choi, Y. J.; Yang, J.-M.; Ham, S.; Jeon, S. K.; Lee, J. Y.; Song, Y.-H.; Ji, E. K.; Yoon, D.-H.; Seo, S.; Shin, H.; Han, G. S.; Jung, H. S.; Kim, D.; Park, N.-G., In-Situ Formed Type I Nanocrystalline Perovskite Film for Highly Efficient Light-Emitting Diode. *ACS Nano* **2017,** *11* (3), 3311-3319.
35. Shi, Y.; Xi, J.; Lei, T.; Yuan, F.; Dai, J.; Ran, C.; Dong, H.; Jiao, B.; Hou, X.; Wu, Z., Rubidium Doping for Enhanced Performance of Highly Efficient Formamidinium-Based Perovskite Light-Emitting Diodes. *ACS Applied Materials & Interfaces* **2018,** *10* (11), 9849-9857.
36. Ling, Y.; Tian, Y.; Wang, X.; Wang, J. C.; Knox, J. M.; Perez-Orive, F.; Du, Y.; Tan, L.; Hanson, K.; Ma, B.; Gao, H., Enhanced Optical and Electrical Properties of Polymer-Assisted All-Inorganic Perovskites for Light-Emitting Diodes. *Advanced Materials* **2016,** *28* (40), 8983-8989.
37. Zhao, X.; Zhang, B.; Zhao, R.; Yao, B.; Liu, X.; Liu, J.; Xie, Z., Simple and Efficient Green-Light-Emitting Diodes Based on Thin Organolead Bromide Perovskite Films via Tuning Precursor Ratios and Postannealing Temperature. *The Journal of Physical Chemistry Letters* **2016,** *7* (21), 4259-4266.
38. Zou, Y.; Ban, M.; Yang, Y.; Bai, S.; Wu, C.; Han, Y.; Wu, T.; Tan, Y.; Huang, Q.; Gao, X.; Song, T.; Zhang, Q.; Sun, B., Boosting Perovskite Light-Emitting Diode Performance via Tailoring Interfacial Contact. *ACS Applied Materials & Interfaces* **2018,** *10* (28), 24320-24326.